International Journal of Fatigue 159 (2022) 106729

Contents lists available at ScienceDirect

International Journal of Fatigue

journal homepage: www.elsevier.com/locate/ijfatigue

Obtaining a lower estimate of the fatigue limit of metals by a simplified quantitative thermometric approach in a low-cost one-specimen test

Florian Schaefer [a,*], Jan Rosar [a], Haoran Wu [b,c], Peter Starke [c], Michael Marx [a]

[a] Department of Materials Science and Methods, Saarland University, Saarbruecken, 66123, Germany
[b] Faculty of Natural Sciences and Technology, Saarland University, Saarbruecken, 66123, Germany
[c] Department of Materials Science and Materials Testing, University of Applied Sciences Kaiserslautern, Kaiserslautern, 67659, Germany

ARTICLE INFO

Keywords:
Quantitative thermometry
Fatigue limit
NTCs
Thermography
One-specimen test

ABSTRACT

The plasticity of metals leads to an internal heat generation during fatigue testing. Therefore, qualitative and quantitative thermography are widely accepted for assessing fatigue damage. The onset of significant heat generation and temperature rise is usually attributed to the fatigue limit of a material. Now, a 40-year-old but just rarely used measurement technique using NTC thermistors is used to reveal the temperature profile in a specimen. A direct comparison with modern thermographic methods exposes the much higher resolution of this simple and inexpensive method. This method provides the much desired ability to assess fatigue limit rapidly and efficiently with only one specimen, even for homogeneous materials and materials conditions with high thermal conductivity or even for small specimen volumes, in a valid and very reliable manner.

1. Introduction

Fatigue damage of metals is by nature a progressive process of ongoing reversible and irreversible deformation and damage accumulation. Fatigue testing becomes more critical the closer one moves from high load amplitudes and few cycles to failure (LCF, low cycle fatigue) into the fatigue limit regime (HCF, high cycle fatigue), because the crack initiation phase becomes more and more life-determining [1].

However, the crack initiation phase is afflicted by a large statistical scatter. Therefore, to determine the fatigue limit, a large number of specimens must be tested for a very high number of load cycles. At the same time, the test frequency is often limited by strain rate effects or severe specimen heating up through dissipation processes within the plastically deformed microstructure. In combination, this leads to disproportional costs just to determine one material parameter, the fatigue limit. The standard methods are very time-consuming and as a results, an efficient material development might be delayed. Therefore, the one-specimen test for the fatigue limit is like the holy grail of fatigue testing.

For this purpose, it is necessary to detect a change in the specimen, i.e. to obtain a signal from the specimen that clearly indicates when fatigue damage starts. Static material parameters as the yield strength are not easily transferable because long before the macroscopic yield strength is reached, microplasticity already occurs, which can accumulate into damage during fatigue. The well-known Bauschinger effect [2] makes this also clear beyond doubt.

Plastic deformation leads to irreversible changes in the microstructure of a material. This irreversibility becomes evident in the stress–strain hysteresis. In the LCF case, the hysteresis loop area is large and easy to measure just e.g. with a standard clip-on extensometer. But, in the HCF regime, that is characterized by global elastic and just local plastic behavior, it is hardly possible to determine the hysteresis loop area with the measuring and testing techniques known at present. Since the irreversible deformation work is essentially heat dissipated [3] (see. Section 2), it is obvious to use thermometry to determine the quantitative amount of heat generated per unit volume and per oscillation cycle and contrast it to the stress amplitude applied.

The correlation of damage and the evolution of the specimen temperature is not new. In 1914, C. E. Stromeyer attempted to relate the fatigue limit of steel to the dissipated energy. For this purpose, he determined the change in temperature of water, which he let flow continuously through a sample [4]. Until the 1950s, there were a large number of publications regarding the correlation of thermometry, energy dissipation and fatigue limit [5]. As the resolution of temperature senors increased, the measurement accuracy of thermometry improved significantly.

Basic work on the combination of an incremental load increases test (LIT) with quantitative thermometry (QT) using thermistors with negative temperature coefficient (NTCs) was done by Klaus Staerk, but only published in German [6,7]. Although no one has continued up his

* Corresponding author.
E-mail addresses: f.schaefer@matsci.uni-sb.de (F. Schaefer), haoran.wu@uni-saarland.de (H. Wu), peter.starke@hs-kl.de (P. Starke), m.marx@matsci.uni-sb.de (M. Marx).

https://doi.org/10.1016/j.ijfatigue.2022.106729
Received 3 September 2021; Received in revised form 14 December 2021; Accepted 7 January 2022
Available online 4 February 2022

seminal work, the resolution of his method is unsurpassed to this day as shown in the following sections.

In the following years, the measurement of the temperature rise in the middle of the strut of a specimen compared to the specimen shoulders, mostly tempered by thermostats, came to the fore, mainly for axial tension. The simple use of new thermographic cameras compared to thermocouples and NTCs promoted this method. However, the limited thermal resolution of thermography and thermocouples with some 10 mK is several orders of magnitude worse than the thermal resolution of NTCs.

The common meaning quickly developed that damage is accompanied by an initial temperature rise in the center of the specimen [8] and that a temperature rise below the fatigue limit is negligible [9]. Up to the onset of localized failure, Meneghetti stated in 2007 that under the assumption that the temperature in the center of the specimen were a suitable parameter for describing the fatigue behavior, the specimen should also always fail there [10]. But, this is known not to be the case. Excluding inhomogeneities in the specimen material, the temperature in the center of the specimen can, however, be determined as an approximation for the curvature of the temperature profile, on the supposition that the boundary conditions, i.e. the temperature at the clamping, and so the heat conduction, are symmetrical.

Guo et al. achieved a breakthrough in 2015 by fitting the temperature profiles from a high-resolution thermographic measurement with the steady-state solution of the heat equation [11]. Like Klaus Staerk already reported in 1982, they were able to show that significant heat is already generated during the LIT even at load steps below the fatigue limit. This non-damaging heat generation can be attributed to anelastic effects such as the Snoek effect [12] or dislocation oscillation [13].

However, the aim of this study is to reveal the benefits of QT using thermistors in the direct comparison with thermographic methods. The evaluation based on a simplified heat equation is contrasted to a more complex evaluation based on curve fitting. The limitations and challenges of the methods are highlighted.

2. Materials and methods

2.1. Thermodynamic background

From the mechanical and thermodynamic point of view, fatigue is usually considered as a dissipative, quasi-static process. Most of the dissipated energy is released as thermal energy, considered as heat generation, causing the temperature of the material to increase.

Combining the first and the second principles of thermodynamics provides the heat equation assuming the mass density $\rho = \rho(\mathbf{r},t) = const.$ and heat capacity $C = C(\mathbf{r},t) = const.$ being material constants and independent of the thermodynamic state and $T = T(\mathbf{r},t)$ being the temperature at a point $\mathbf{r}$ at time t [14] gives

$$\rho C\dot{T} - \nabla\,(k(\mathbf{r})\nabla T) = d_1(\mathbf{r},t) + s_{the}(\mathbf{r},t) + s_{ic}(\mathbf{r},t) + r_{ext}(\mathbf{r},t) \tag{1}$$

with the material's heat conduction tensor k, the internal coupling source s_{ic}, the external heat supply r_{ext}, the thermoelastic source s_{the} and the mechanical dissipation source d_1. The left-hand side of Eq. (1) describes a second-order linear differential equation of the temperature whereas the right-hand-side groups all the heat supplies to the thermodynamic state of the system. Considering the system with the Helmholtz free energy Ψ as its thermodynamic potential in an equilibrium state the system is characterized by a set of state variables being T, the strain tensor ε as the sum of the elastic and plastic strain tensors $(\varepsilon_{el} + \varepsilon_{pl})$ and a vector of n internal variables α_i. Then the intrinsic mechanical dissipation source $d_1(\mathbf{r},t)$ is

$$d_1 = \left(\sigma - \rho\frac{\partial\Psi}{\partial\varepsilon_{el}}\right) : \dot{\varepsilon}_{el} - \rho\frac{\partial\Psi}{\partial\alpha}\cdot\dot{\alpha} \tag{2}$$

The thermoelastic effect generates heat as

$$s_{the} = \rho T\frac{\partial^2\Psi}{\partial T\partial\varepsilon_{el}} : \dot{\varepsilon}_{el} \tag{3}$$

The internal coupling source is

$$s_{ic} = \rho T\frac{\partial^2\Psi}{\partial T\partial\alpha}\cdot\dot{\alpha} \tag{4}$$

The internal coupling source s_{ic} is assumed to vanish because an effect of the fatigue on the microstructural state can be neglected for the small temperature changes in this investigation before crack initiation. Hence, fatigue is considered to be a purely dissipative process [15].

The external heat supply r_{ext} is considered to be time-independent and is vanishing [14,16]. The heat conduction tensor is assumed to be constant, even for changes in temperature, $k_{ij} = k\delta_{ij}$ hence Eq. (1) simplifies to

$$\rho C\frac{\partial\theta}{\partial t} - k\Delta\theta = s = s_{the} + d_i \tag{5}$$

Here Δ denotes the Laplace operator and θ the temperature variation $T - T_0$.

The heat source estimation throughout a 3D specimen is an ill-posed problem and hence it is impossible to solve without information on the heat source distribution. Boulanger et al. assumed that the surface temperature equals the average depth-wise temperature distribution and so, a mean heat source over each specimen cross section [14]. Integrating Eq. (5) delivers

$$\rho C\left(\frac{\partial\theta}{\partial t} + \frac{\theta}{\tau_{th}^{1D}}\right) - k\frac{\partial^2\theta}{\partial x^2} = s \tag{6}$$

τ_{th}^{1D} describes the heat exchange through the specimen surface with its surroundings by radiation and convection. In a nutshell, Eq. (6) describes the 1-dimensional temperature profile on the surface of a flat specimen gauge length measurable by thermography in a temperature-controlled room assuming that the surface temperature is representative and that the specimen is not heated up too much during fatigue (no fatigue heat treatment).

If we consider e.g. a sinusoidal load function with the start time t_i of a load cycle i and the frequency f, the terms in Eq. (6) can be averaged.

$$\begin{cases} \bar{d}_1(i) = f\int_{t_i}^{t_i+1/f} d_1(\tau)d\tau \\ \bar{\theta}(x,i) = f\int_{t_i}^{t_i+1/f} \theta(x,\tau)d\tau \\ \int_{t_i}^{t_i+1/f} s_{the}(\tau)d\tau = 0 \\ \int_{t_i}^{t_i+1/f} \frac{\partial\theta(x,\tau)}{\partial\tau}d\tau = 0 \end{cases} \tag{7}$$

Eq. (6) further simplifies to

$$\rho C\frac{\bar{\theta}(x,i)}{\tau_{th}^{1D}} - k\frac{\partial^2\bar{\theta}(x,i)}{\partial x^2} = \bar{d}_1(i) \tag{8}$$

For a given load cycle i, Eq. (8) is a second-order linear differential equation with coordinate-independent coefficients. The general solution is of kind

$$\bar{\theta}(x,i) = A_1(i)e^{bx} + A_2(i)e^{-bx} + A_3(i) \tag{9}$$

with

$$A_3(i) = \frac{\tau_{th}^{1D}\bar{d}_1(i)}{\rho C} \tag{10}$$

and

$$b = \sqrt{\frac{\rho C}{k\tau_{th}^{1D}}} \tag{11}$$

So, the heat generated per load cycle q is given by

$$q = \frac{kb^2A_3(i)}{f} \tag{12}$$

and can be evaluated by a 1D linear regression fit of the temperature profile of the sample gathered by thermography. If the temperature profile is not measured by thermography, the specimen surface can be thermally isolated using e.g. foamed up polyurethane. Then τ_{th}^{1D} tends

to infinity because temperature exchanges with the specimen's surroundings by convection and radiation vanish. Eq. (8) further simplifies to

$$\bar{d}_1(i) + k\frac{\partial^2\bar{\theta}(x,i)}{\partial x^2} = 0 \tag{13}$$

A simple polynomial solution is given by

$$\bar{\theta}(x,i) = -\frac{\dot{q}}{2k}x^2 + mx + n \tag{14}$$

For 3 distinct measuring points for the temperatures using NTCs T_1, T_2, T_3, at positions for example s_1 at the lower end of the gauge length, s_2 in the middle and s_3 at the upper end of the gauge length $\dot{q}$ can be determined by [17]

$$q = \dot{q}\cdot\frac{1}{f} = \frac{2k}{f}\frac{(T_3 - T_2)\cdot s_3 + (T_2 - T1)\cdot s_1}{s_1 s_3(s_3 - s_1)} \tag{15}$$

Using 5 measuring point can further improve the fit to the temperature profile assumed to be parabolic but this evaluation is not part of this study because the specimen tested were too small for more than 3 NTCs.

2.2. Measurement of temperature profiles

Step-wise and continuous LITs were performed using a resonance testing machine Rumul Mikrotron from Russenberger Pruefmaschinen AG, Neuhausen am Rheinfall, Switzerland. The specimens were tested with stress ratios R of 0.1 and -1.

If the load amplitude increases, the specimen temperature (in the middle) initially rises, but reaches a steady-state value after a minimum number of load cycles [10,16]. The number of load cycles at each load step was chosen to achieve this steady-state temperature. This temperature is used for evaluating the curvature of the temperature profile and thus for determining the heat generated per load cycle q. q is then assigned to the respective stress amplitude.

All tests were carried out at room temperature of 25 °C.

2.2.1. Temperature profiles from NTCs

The temperature measurements were performed with miniature thermistor from TE (type GAGA10KM3499J15). Due to its small size (< 0.4 mm) and high resolution (±0.01 Ω) compared to its reference resistance of 10 kΩ, a very local detection of the temperature with outstanding temperature resolution is possible. Since NTCs have a variance in their characteristic curves, a temperature-resistance calibration had to be carried out for each thermistor. The reacting time of these small NTCs is below 1 s and allows even for fast measurements without a noteworthy delay.

In order to calibrate the NTCs, the NTCs were packed inside small polymer foil bags and immersed in tempered water in a thermostat bath. The temperature of the water bath is additionally measured by a calibrated high resolution mercury thermometer. A temperature range of 25 °C to 45 °C was selected for the water temperatures. The temperature was adjusted in steps of about 5 °C.

The characteristic equation is calculated according to

$$\frac{1}{T(R)} = A' + B'\ln\left(\frac{R}{R_0}\right) + C'\ln\left(\frac{R}{R_0}\right)^2 + D'\ln\left(\frac{R}{R_0}\right)^3 \tag{16}$$

with R being the electric resistance at temperature T and R_0 the reference resistance at 25 °C.

Since only a very small temperature increase occurs when the fatigue limit is exceeded, the characteristic curve can be linearized. This was done with by a Taylor series at the starting temperature, which is finished after the linear term (see Fig. 1). As a result, the measurements errors increases for the high stress amplitudes. For the fatigue limit regime, the temperature increase is that small, that an error of less than 1% can be ignored (see Fig. 2).

When applying the NTCs, special care must be taken to ensure that the fatigue strength is not impaired and that a support as stable as possible is created. The thermistors were applied to flat tensile specimens in form of a layered composite. This provides the advantage that the composite could easily be re-used for a number of tests and specimens.

For this purpose, an electrical insulating Mylar foil was glued to the specimen surface with a thin layer of cyanoacrylate. The insulating foil must be as thin as possible to achieve a fast reacting time. The three NTCs were then applied to the film using double-sided adhesive tape. To protect the NTCs, another layer of insulating film was then applied (Fig. 3). For the round tensile specimens, the application was carried out by a layer of insulating foil and by embedding the NTC in adhesive tape. The specimens with the adapted NTCs were thermally isolated using foamed up polyurethane pipe insulants.

The electrical resistances of the NTCs were measured using standard digital multimeters, Keithley DMMs with a resolution of less than

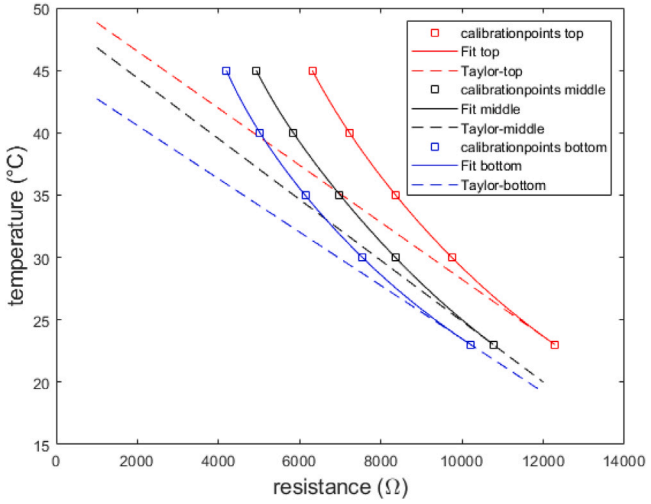

Fig. 1. Fit of Eq. (16) to calibration data sets of temperature and electrical resistance of 3 NTCs on one specimen to get the characteristic curve. The Taylor series approximation is added.

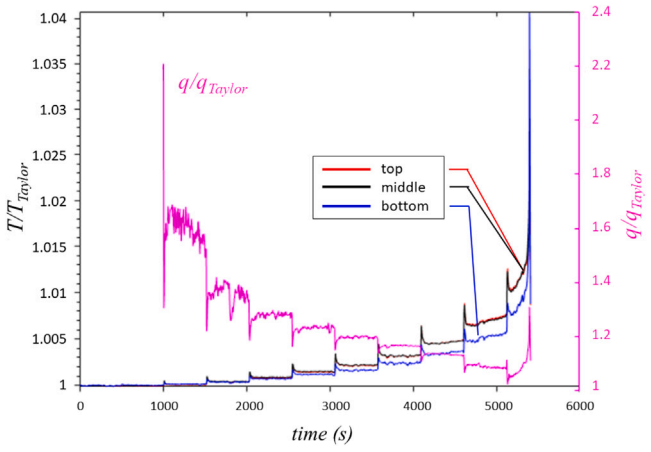

Fig. 2. Comparison of the temperature calculated by Eq. (16) T and the approximation by a Taylor series T_{Taylor} for the NTCs at the top and bottom position (red, blue line) and the middle position (black line) of a coarse-grained Ni specimen. The bottom temperature is below the top temperature in all tests carried out because the heat conduction boundary conditions were asymmetrical for our testing setup at the resonance testing machine. The calculated error for the heat generated per load cycle q from Eq. (15) by using the Taylor approximation. The temperature evolution for each load step of the step-wise LIT indicates cyclic softening. (For interpretation of the references to color in this figure legend, the reader is referred to the web version of this article.)

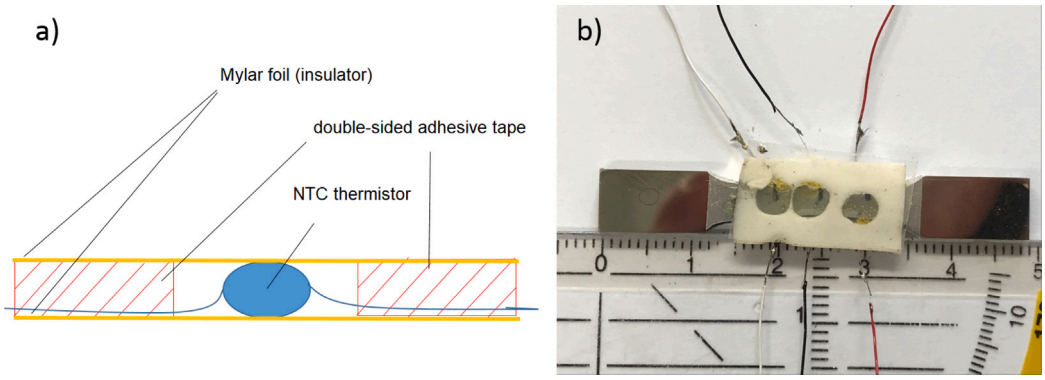

Fig. 3. NTC setup for attachment to the specimens, (a) schematic and (b) fixed to a flat tensile specimen.

10 mΩ, readout with LabVIEW® via a GPIB2USB adaptor. The data evaluation was done with MATLAB®.

2.2.2. Thermography

Thermographic images were acquired with 1 fps and 382 x 288 pixel^2 in the full window mode with an infrared imaging system (Micro-Epsilon thermoIMAGER TIM 450) with a thermal sensitivity of 0.04 K at room temperature. In order to have a good emissivity the specimens' surface was coated with graphite spray. To have stable temperature conditions and to reduce heat conduction and interference radiation, the setup was shielded using paper fleece sheets.

The temperature profiles along the specimens' gauge length resulted from averaging the temperature data along the width of the flat tensile specimens.

2.3. Materials

For the fatigue tests, macro-round tensile specimens were prepared from S235JR (1.0038 steel) and 1.0314 steel and flat tensile specimens from S235JR. Flat specimens from Ni serve as reference material for calibration measurements. All specimen geometries were designed according to ASTM standard E466-07.

Noteworthy microstructural changes in the materials due to heating up during fatigue can be excluded because the maximum temperature during fatigue was well below 30 % of the homologous temperature.

All specimens were ground and polished to 1 µm using SiC papers and polycrystalline diamond polishing suspensions to avoid an influence of the specimen's surface state on the crack initiation and therefore, the fatigue strength.

3. Results

The results from the thermographic temperature profile measurement are shown in Fig. 4. The double-exponential fit from Eq. (12) is in very good agreement with the raw temperature data, averaged along the specimen width in order to reduce noise.

Fatigue of metals results in an advancing increase in temperature in the middle of a tensile specimen and, due to thermal conduction to the specimen's shoulders and to the clamping, in a parabolic or double-exponential temperature profile (see Figs. 5 and 4). In case of asymmetrical thermal boundary conditions, such as un-cooled clampings, the profiles are asymmetrical concerning the specimen's geometry. If the thermal conductivity is high, the increase of temperate is less pronounced due to a large heat flux. If the specimen is small, less heat is generated and the increase in temperature is also small. Since the specimen temperature follows directly from the heat generated per load cycle and the heat loss through heat flux per time, the temperature in the middle of the specimen also decreases with decreasing test frequencies. Hence, for small specimens even with a parallel length of

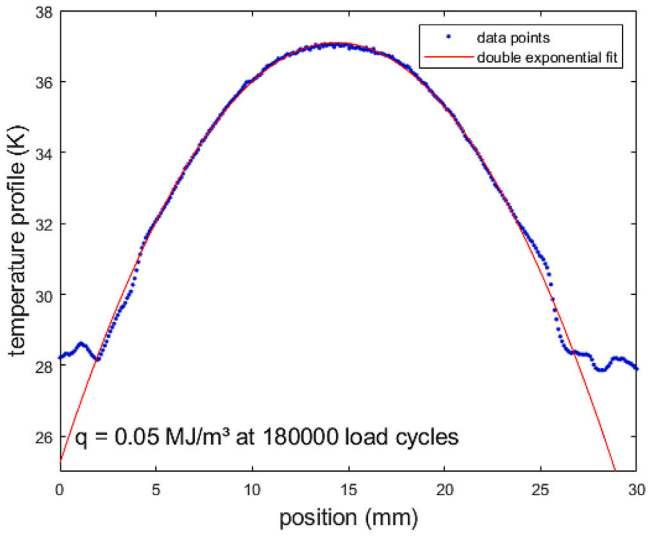

Fig. 4. Temperature profile at 180 000 load cycles for coarse-grained Ni measured by thermography, averaged along the specimen width. A double-exponential fit is in good agreement with the raw temperature data. q follows from Eq. (12).

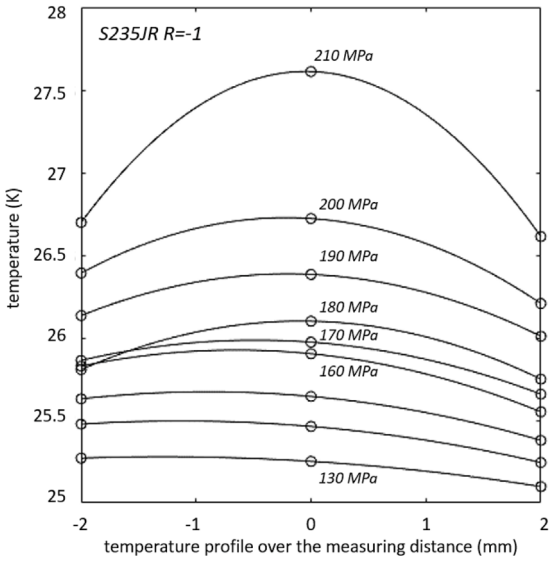

Fig. 5. Evolution of the specimen steady-state temperature of S235JR steel measured at 3 distinct points by NTCs during LIT, interpolated by Eq. (14), profiles are shown for stress levels between 130 MPa and 210 MPa in steps of 10 MPa.

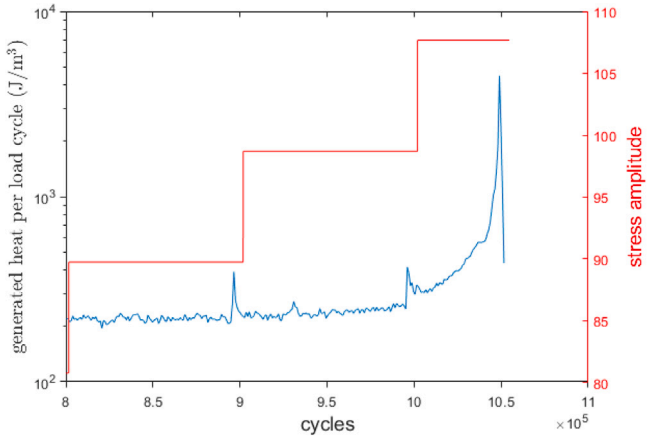

Fig. 6. $\sigma_a - q$ data from 1.0314 steel at $R = -1$, cyclic softening is visible in each load step (red curve) from an severe increase in q after a load increase, followed by a relaxation to the steady-state. After the transition to failure accumulation, no steady-state is reached during the last step, the last 10^5 load cycles. (For interpretation of the references to color in this figure legend, the reader is referred to the web version of this article.)

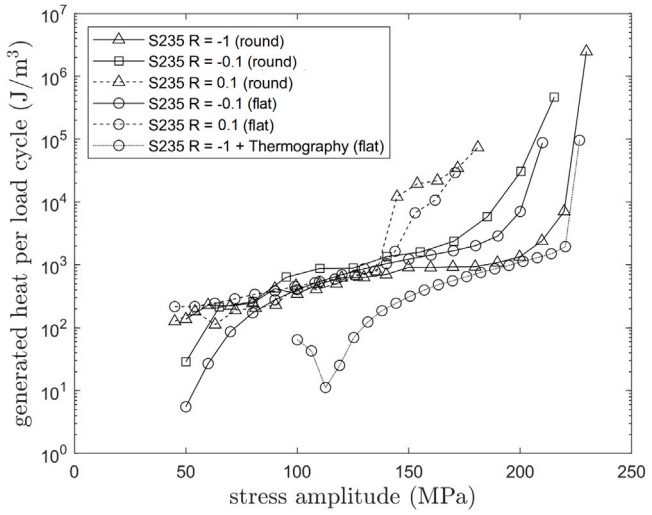

Fig. 7. Comparison of the stress amplitude σ_a with the steady-state heat generated per load cycle q from a staircase test (LIT) for S235JR steel for flat and round specimens and for different R values. For $R = 0.1$ a jump in q becomes evident due to the onset of plasticity at the upper yield point followed by softening (lower yield point).

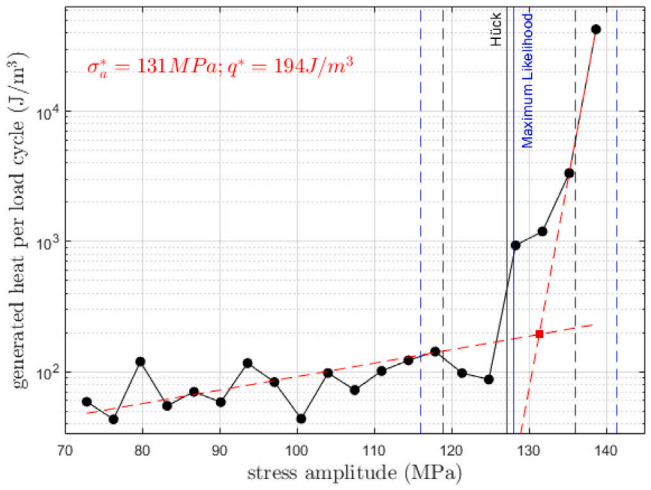

Fig. 8. Direct comparison of the knee-stress amplitude σ_a^* with the fatigue limit estimate from a staircase test, analysis following Hueck and by maximum-likelihood method (incl. scattering bands) for 1.0314 steel.

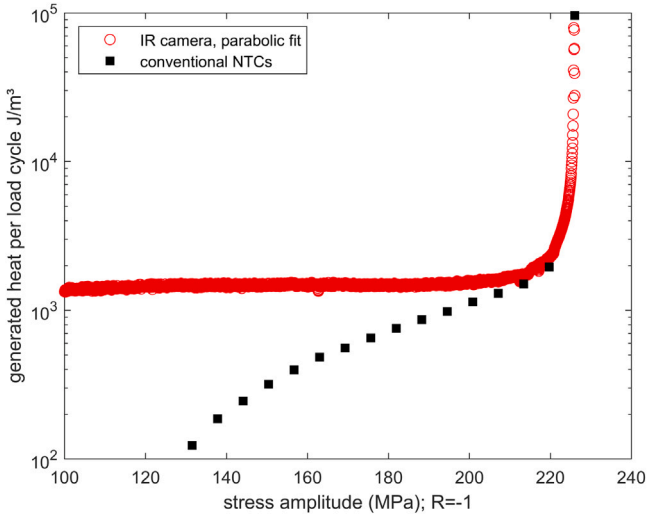

Fig. 9. Evolution of heat generated per load cycle, measured by the NTC method (Eq. (15)) and by thermography (Eqs. (8)–(12)) for coarse-grained Ni.

less than 10 mm, low test frequencies (even for servohydraulic testing systems) and for metals with high thermal conductivity of the material such as Al, the NTC method is the method of choice.

If the stress amplitude σ_a and the heat generated per load cycle q are contrasted (Fig. 6), the knee-point stress amplitude σ_a^* becomes evident (see Figs. 7 and 8).

Fig. 7 shows the $\sigma_a - q$ curves for the S235JR steel specimens, whereas q denotes the steady-state value prior each load increase step. It is remarkable that, regardless of the R value, the transition value of q is the same, i.e., damage appears to start by a process that leaves a characteristic fingerprint in the heat generation. The specimens tested at $R = 0.1$ show an abrupt increase that can be attributed to the yield strength effect. When the upper yield strength is reached, cycling softening occurs and the heat generation increases through the easy dislocation slip. If $R < 0$ cyclic hardening leads to a continuous increase in heat generation.

4. Discussion

4.1. Validity of thermodynamic equations

With a temperature increase of less than 5 °C in the middle of the specimen up to the fatigue limit regime, only a deviation in the determination of q of less than 1 % is expected, originating from the non-constant coefficient of thermal conductivity $k(T)$ as shown by Staerk et al. [7].

The knee-stress amplitude σ_a^* is computed from the heat generated per load cycle in the steady-state regime of each load step in the LIT q and the corresponding stress amplitude σ_a levels. During the iterative procedure, the logarithmized value-pairs are divided into 2 classes and within the classes, linear regression is used to determine the slope of the curve. σ_a^* is estimated as the stress amplitude at which the classes are divided in such a way that the change in the slope of the regression lines becomes maximum (Fig. 8).

Fig. 9 reveals that, in a direct juxtaposition of the measured generated heat per load cycle q from thermography and estimated by the NTC method, the thermography suffers from the comparable lower

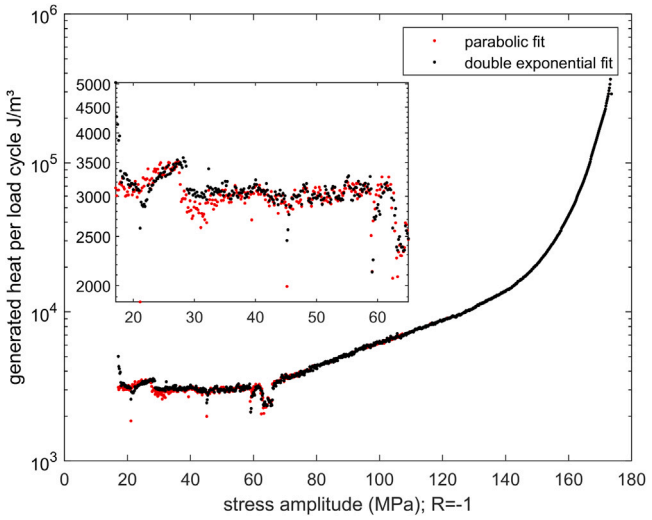

Fig. 10. Direct comparison of $\sigma_a - q$ data, measured by thermography and calculated by Eq. (8) (Guo et al. exponential fit) and Eq. (15) (Staerk et al. parabolic fit). Deviations between both curves are just visible in the lower part on the left-hand side.

resolution resulting in temperature scattering and a higher zero-level of q. Although the resolution is worse, the knee-stress amplitude is also determinable as the onset of the curve instead of a knee-point. However, it is not undoubted if the knee-point can be determined even for materials which request a higher resolution due to a higher thermal conductivity, a smaller sample size or for testing with lower frequencies. These parameters result in less increase in temperature and therefore, the transition point might be transcended using thermography.

Apart from all questions concerning the resolution of the thermography, it is nevertheless striking that in the upper part both curves coincide. Although the NTCs were operated without additional thermal isolation, due to the simultaneous thermographic measurement, no significant differences in the results are observable. Comparing the thermographic evaluation according to Guo et al. using Eqs. (8)–(12) with the evaluation according to Eq. (15), no significant difference in the determined generated heat per load cycle are visible (Fig. 10). This underlines that even without thermal isolation of the specimen, influences due to radiation and convection can be neglected. τ_{th}^{1D} thus tends to infinity. For our experiment the evaluation based on the simplified heat Eq. (13) is redundant to using Eq. (8).

4.2. The knee-stress amplitude σ_a^*, an estimate for the fatigue limit?

The $\sigma_a - \dot{q}$-curve is obviously divided into two regimes. It is reasonable to correlate the knee-point between both with the fatigue limit. In the lower stress regime, the fatigue-resistant regime, heat generation is assumed to be due to anelastic effects such as the Snoek effect, the Zener mechanism or dislocation oscillations [13]. The temperature rise is explained by the heat generation from the emission of acoustic waves during oscillations of dislocation segments [18].

In the region of high Morrow exponents, the finite-life fatigue regime, the higher energy dissipation occurs due to dislocation motion, which can lead to damage in the interplay between strain accumulation and progressive dislocation immobilization [19,20]. In the popular view, the energy dissipation beyond σ_a^* is associated with the formation of persistent slip bands (PSB) [21].

Stanzl-Tschegg et al. showed that even below the plastic strain amplitude $\varepsilon_{a,p}$ at which PSBs occur in conventional HCF testing, localized PSBs already occur in the very-high-cycle fatigue (VHCF) regime during ultrasonic fatigue testing. Furthermore, although PSB formation leads to a measurable hysteresis loop, in the VHCF range the fatigue limit is about twice the threshold value of the plastic strain amplitude ε_a for PSB formation [22].

This highlights the fact that the mechanisms underlying the knee-point in the $\sigma_a - \dot{q}$-curve are only beginning to be understood and that a more detailed consideration is needed in the future.

However, σ_a^* describes the onset of cyclic plastic deformation, not everywhere in the specimen but at least at some localized spots. If this contributes to damage is not imperative. But, σ_a^* is with certainty, a lower estimate for the fatigue limit.

4.3. Correlation with the finite-life fatigue strength

During fatigue, the magnitude of plastic strain amplitudes $\varepsilon_{a,p}$ is affected by both, microstructural changes and potential crack opening and by crack growth effects. Therefore, $\varepsilon_{p,a}$ consequently does not allow discrimination between these mechanisms. However, if one additionally considers the temperature and the electrical resistance of the specimen (material separations = cracking), a separation of the damage mechanisms is possible, if necessary.

If we exclude cracking, the temperature increase arises essentially from the work of plastic deformation W [3]. Introducing a hysteresis form factor F for the stabilized state of the mechanical hysteresis, an estimate of the total area of the hysteresis loop, the work per cycle ΔW becomes to

$$\Delta W = F \cdot \varepsilon_{p,a} \cdot \sigma_a \tag{17}$$

The Morrow equation, Eq. (18), for the cyclic hardening [23] is based on the Ramberg–Osgood equation and is

$$\sigma_a = k' \cdot \varepsilon_{p,a}^{n'} \tag{18}$$

with the cyclic hardening coefficient k' and the cyclic hardening or Morrow exponent n'. Combining Eqs. (17) and (18) delivers

$$\sigma_a = \left(\frac{k'}{F^{n'}}\right)^{\frac{1}{1+n'}} \Delta W^{\frac{n'}{1+n'}} \tag{19}$$

If we assume that a constant (and large) fraction of the work of deformation is dissipated as heat, a constant temperature profile is formed under the assumption of constant thermal conductivity and constant thermal boundary conditions (see Section 2). Therefore, it follows

$$\sigma_a = const. \cdot \Delta T^{\frac{n'}{1+n'}} \tag{20}$$

With the exception of the time immediately after the start of a test or after a load amplitude increase step in a LIT, the work of deformation, and hence the temperature profile, always becomes stationary. Thus, the knee-value of the stress amplitude in the LIT σ_a^* can be directly correlated with a change in the Morrow exponent n'.

The Morrow exponent in the finite-life fatigue regime is the parameter to identify with the aim to determine the SN curve from the QT data. By default, ΔT or a corresponding damage parameter is measured on one specimen at 3 points in a LIT using cooled clamps. An additional constant amplitude fatigue test (CAT) was performed to check for effects of thermal conductivity and of the load history during the LIT [24,25]. The slope b of the Basquin equation

$$N_f = 0.5\left(\frac{\sigma_a}{\sigma_a^*}\right)^{-b} \tag{21}$$

for the numbers of load cycles to failure N_f that describes the finite-lifetime regime follows from the Morrow Eq. (18) as

$$b = \frac{n'}{5n'+1} \tag{22}$$

This procedure has already been published by Starke et al. as the physically based fatigue life calculation method PHYBAL [24–26]. Hence, using QT to determine the knee-stress amplitude σ_a^* in a LIT allows to evaluate the whole SN curve. If effects from the load history are present, two additional tests are needed (CAT) to correct n'. So, QT can be extended to the evaluation of the finite-lifetime regime (see Fig. 11).

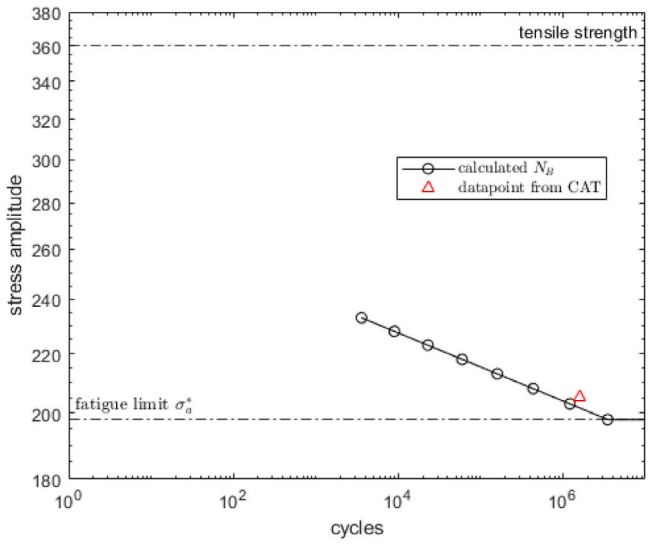

Fig. 11. Combination of fatigue limit estimate as the knee-stress amplitude from QT and a short-time evaluation of the finite-lifetime regime. The CAT shows good agreement with the results of the LIT. Hence, effects from the load history during the LIT are disregarded. Therefore, a second CAT is omitted.

5. Conclusion

Quantitative thermography allows to elucidate the evolution of heat generation during fatigue. Thereby, deformation mechanisms seem to a show characteristic heat generation per load cycle. The experimental results are highly reproducible.

It is shown that classical thermometry is superior to thermography in temperature measurement due to the higher temperature resolution of the sensors. It has been shown that elaborate thermal isolation of the specimens is unnecessary because radiation and convection have only a negligible contribution to the overall heat flux as long as the specimen thermal boundary conditions are not too asymmetric or the temperature difference between the clamps is not higher than the specimen heating up.

QT using thermography is the easy method of choice for materials with low thermal conductivity, with large sample volume and at high frequencies. However, one must be able to exclude strain rate effects. QT with NTCs helps to expand the limits of thermography.

In addition to the QT, the damping of the material [27] e.g. in resonance fatigue testing can be considered as a further parameter for determining the fatigue limit. A combination of both methods can provide further information about the underlying deformation mechanism in future investigations.

Declaration of competing interest

The authors declare that they have no known competing financial interests or personal relationships that could have appeared to influence the work reported in this paper.

Acknowledgments

We thank Marc Schmidt from the Technical University Kaiserslautern for providing the data for the fatigue limit of the material C2C during his master thesis at FuWe of Saarland University. We thank Jonas Rauber from MWW for proof-reading. We are indebted to Christian Motz from MWW at Saarland University for providing his facilities for this project. We acknowledge the financial support from Saarland for the resonance testing machine, Germany (DFG INST 256/500-1 LAGG).

References

[1] Goto M. Scatter characteristics of fatigue life and the behaviour of small cracks. Fatigue Fract Eng Mater Struct 1992;15(10):953–63.
[2] Bauschinger J. Über die veränderung der elastizitätsgrenze und der festigkeit des eisens und stahls durch strecken und quetschen, durch erwärmen und abkühlen und durch oftmals wiederholte beanspruchung. Mitt Mech-Tech Lab K Tech Hochsch Münch 1886;13(1).
[3] Biallas G, Piotrowski A, Eifler D. Cyclic stress-strain, stress-temperature and stress-electrical resistance response of NiCuMo alloyed sintered steel. Int J Fatigue 1996;6(18):419.
[4] Stromeyer C. The determination of fatigue limits under alternating stress conditions. Proc R Soc Lond Ser A Contain Pap Math Phys Charact 1914;90(620):411–25.
[5] Dengel D, Harig H. Estimation of the fatigue limit by progressively-increasing load tests. Fatigue Fract Eng Mater Struct 1980;3(2):113–28.
[6] Staerk KF. Einsatz von heißleiter-temperaturfühlern in der werkstoffprüfung. Materwiss Werksttech 1982;13(9):309–13.
[7] Staerk KF. Temperaturmessung an schwingend beanspruchten werkstoffen. Materwiss Werksttech 1982;13(10):333–8.
[8] Luong MP. Fatigue limit evaluation of metals using an infrared thermographic technique. Mech Mater 1998;28(1–4):155–63.
[9] La Rosa G, Risitano A. Thermographic methodology for rapid determination of the fatigue limit of materials and mechanical components. Int J Fatigue 2000;22(1):65–73.
[10] Meneghetti G. Analysis of the fatigue strength of a stainless steel based on the energy dissipation. Int J Fatigue 2007;29(1):81–94.
[11] Guo Q, Guo X, Fan J, Syed R, Wu C. An energy method for rapid evaluation of high-cycle fatigue parameters based on intrinsic dissipation. Int J Fatigue 2015;80:136–44.
[12] Snoek J. Effect of small quantities of carbon and nitrogen on the elastic and plastic properties of iron. Physica 1941;8(7):711–33.
[13] Mareau C, Favier V, Weber B, Galtier A, Berveiller M. Micromechanical modeling of the interactions between the microstructure and the dissipative deformation mechanisms in steels under cyclic loading. Int J Plast 2012;32:106–20.
[14] Boulanger T, Chrysochoos A, Mabru C, Galtier A. Calorimetric analysis of dissipative and thermoelastic effects associated with the fatigue behavior of steels. Int J Fatigue 2004;26(3):221–9.
[15] Morabito A, Chrysochoos A, Dattoma V, Galietti U. Analysis of heat sources accompanying the fatigue of 2024 T3 aluminium alloys. Int J Fatigue 2007;29(5):977–84.
[16] Teng Z, Wu H, Boller C, Starke P. Thermography in high cycle fatigue short-term evaluation procedures applied to a medium carbon steel. Fatigue Fract Eng Mater Struct 2020;43(3):515–26.
[17] Staerk K. Thermometrische untersuchungen zum zyklischen verformungsverhalten metallischer werkstoffe (Dissertation Universität Stuttgart, Ph.D. thesis), IWMF Stuttgart; 1980.
[18] Maquin F, Pierron F. Heat dissipation measurements in low stress cyclic loading of metallic materials: From internal friction to micro-plasticity. Mech Mater 2009;41(8):928–42.
[19] Connesson N, Maquin F, Pierron F. Dissipated energy measurements as a marker of microstructural evolution: 316 L and DP600. Acta Mater 2011;59(10):4100–15.
[20] Schäfer F, Lang EP, Bick M, Knorr AF, Marx M, Motz C. Assessing the intergranular crack initiation probability of a grain boundary distribution by an experimental misalignment study of adjacent slip systems. Proc Struct Integr 2017;5:547–54.
[21] Cugy P, Galtier A. Microplasticity and temperature increase in low carbon steels. In: Proceedings of the 7th int. fat. conf., Stockholm (Sweden). 2002.
[22] Stanzl-Tschegg SE, Schönbauer B. Mechanisms of strain localization, crack initiation and fracture of polycrystalline copper in the VHCF regime. Int J Fatigue 2010;32(6):886–93.
[23] Morrow J. Cyclic plastic strain energy and fatigue of metals. In: Internal friction, damping, and cyclic plasticity. ASTM International; 1965.
[24] Starke P, Walther F, Eifler D. PHYBAL—A New method for lifetime prediction based on strain, temperature and electrical measurements. Int J Fatigue 2006;28(9):1028–36.
[25] Starke P, Wu HR, Boller C. Advanced evaluation of fatigue phenomena using non-destructive testing methods. In: Materials science forum, Vol. 879. Trans Tech Publ; 2017, p. 1841–6.
[26] Starke P, Walther F, Eifler D. "PHYBAL" A short-time procedure for a reliable fatigue life calculation. Adv Energy Mater 2010;12(4):276–82.
[27] Mortezavi V, Haghshenas A, Khonsari M, Bollen B. Fatigue analysis of metals using damping parameter. Int J Fatigue 2016;91:124–35.